Comparison of spin relaxation in the metal-hydrogen systems $ZrNiH_x$ and $ZrNiD_x$

Caleb D. Browning,[1] Timothy M. Ivancic,[1] Robert C. Bowman, Jr.,[2] and Mark S. Conradi[1,*]
[1]*Department of Physics, Washington University, CB 1105, One Brookings Drive, St. Louis, Missouri 63130-4899, USA*
[2]*Jet Propulsion Laboratory, California Institute of Technology, Pasadena, California 91190-8099, USA*
(Received 19 October 2005; revised manuscript received 18 January 2006; published 24 April 2006)

Relaxation studies of the intermetallics $ZrNiH_x$ and $ZrNiD_x$ were performed using hydrogen and deuterium NMR in the β ($x \simeq 0.85$) and γ phases ($x \simeq 2.6$ and 3.0). Correlation times for atomic diffusion in the hydride were determined based on the temperature dependence of spin-lattice and spin-spin relaxation times. The hydrogen motion is shown to be thermally activated over the temperature range 300–550 K, and the activation energies for diffusion are determined. The deuterium NMR spectra exhibit incomplete line narrowing with temperature, indicating that the average electric field gradient is not zero when averaged over the deuterium atom sites of these noncubic unit cells. The temperatures of minima in T_1 and T_2 for the deuterides indicate that the motion rates are similar for the D and H systems. However, the activation energies taken from the temperature dependencies of the deuterides' T_1 and T_2 are much smaller than for the hydrides, indicating the deuteride relaxation rates have additional contributions. The spectrum of $ZrNiD_{1.87}$ reveals a coexistence of two phases, in agreement with the phase diagram.

DOI: 10.1103/PhysRevB.73.134113 PACS number(s): 66.30.−h, 76.60.−k, 82.56.−b, 61.50.−f

I. INTRODUCTION

$ZrNiH_x$ is a hydride of an intermetallic compound formed from a good hydriding metal (Zr) and a poor hydriding metal (Ni).[1,2] Thus, the H_2 vapor pressure of the compound[3] at a given temperature is higher than for ZrH_x, for example.[4] The use of intermetallic compounds not only allows some control of the temperature for a given vapor pressure but may permit the storage of hydrogen in lighter weight metals and in less expensive metals.[5,6] The $ZrNiH_x$ system has been used in space applications to release and absorb H_2 gas for gas gap thermal switches.[7] The reliability of the material for this application with its unattended operation has been thoroughly tested.[8,9] ZrNi has also been studied for use as a tritium getter.[10]

The $ZrNiH_x$ system displays a solid-solution phase from $x=0$ to approximately 0.2, according to the published phase diagram.[11] The β phase is stable from $x=0.65$ to nearly 1.0; its structure has an ideal hydrogen content corresponding to $x=1$. Neutron diffraction[2] indicates the hydrogen occupies Zr_4Ni_2 type sites (nearest metal neighbors) in the orthorhombic crystal unit cell, with all sites being chemically (energetically) equivalent. A small triclinic distortion is present. From $x=2.6$ approximately to $x=3.0$, the γ phase occurs at room temperature, with $x=3$ corresponding to completely filled hydrogen sites (per ZrNi formula unit, two Zr_3Ni type sites, and one Zr_3Ni_2 type site). We note that recent thermodynamic measurements[12] have called into question aspects of the $ZrNiH_x$ phase diagram[11] above room temperature.

Adolphi and co-workers have reported deuterium magic-angle spinning (MAS) nuclear magnetic resonance (NMR) results[13] for $ZrNiD_x$. In the γ phase with x near 3, two resonance lines are found with an intensity ratio very near the expected 2:1 [we note that MAS-NMR (Ref. 14) provides angular averaging so that resonances report sets of chemically equivalent nuclei]. In the β phase, two MAS-NMR lines are observed with nearly 1:1 intensity ratio. This provides unambiguous evidence for two different (inequivalent) sets of sites in the β structure, despite the diffraction evidence[2] for a single set of sites (all equivalent). With increasing temperature, in both β and γ phases, the two MAS resonance lines merge or coalesce, allowing a hopping rate to be assigned at that temperature. The narrowing of the nonspinning spectrum[14] and interference of the coherent averaging under MAS by the atomic motion[15,16] provide additional estimates of the hopping rate. Activation energies of diffusion in the β and γ phases were calculated,[13] by assuming typical attempt frequencies.

Except for the MAS deuterium NMR, there is little information reported on the mobility of H or D atoms in the ZrNi hydrides and deuterides. The present work reports T_1 and T_2 relaxation time measurements on the hydride and deuteride in the β and γ phases, and the deuterium spectrum for one mixed phase sample.

II. EXPERIMENTAL METHODS

All $ZrNiH_x$ and most $ZrNiD_x$ samples (except for the sample Knox-5, which was made previously as described in Ref. 13) used for the present NMR studies had been prepared at the Jet Propulsion Laboratory (JPL) in an ultraclean Sieverts-type volumetric apparatus.[17] Very high purity hydrogen or deuterium gas was reacted with pieces cut from a single large (i.e., ~400 g) ingot of high-purity ZrNi intermetallic alloy originally prepared by the Teledyne Wah Chang Company (Albany, OR 97321, USA) using crystal bar purity Zr and Ni metal of comparable purity. The measured composition of this ingot matched the ideal Zr/Ni ratio of 1.0 ± 0.01. Detailed microscopic and x-ray diffraction examinations have been performed by Michel *et al.*[18] on another piece taken from this same ZrNi ingot. They reported the material was almost completely an orthorhombic ZrNi phase with a high density of twinning defects and a minor secondary phase of composition Zr_9Ni_{11}, which lies along the grain boundaries of the host matrix. Chemical analyses were per-

formed at JPL on this ZrNi ingot where the following impurities were found by weight: Fe (130 ppm), O (72 ppm), C (70 ppm), Cu (48 ppm), Mn (23 ppm), N (7 ppm), and no other elements were detected. Other portions of this same ZrNi ingot were also used by (1) Dantzer *et al.*[12] to obtain the hydrogen absorption and desorption isotherms they reported for their sample 2; (2) Prina *et al.*[9] for the preparation and cycling of gas gap heat switches using $ZrNiH_x$; and (3) Adolphi *et al.*[13] for their prior NMR experiments on $ZrNiD_{1.0}$ and $ZrNiD_{3.0}$.

The all-metal Sieverts volumetric system was constructed from electropolished 316L stainless steel tubing and components that were assembled using a combination of orbital welding and various metal-to-metal interface seals to connect valves and pressure sensors.[17] An integrated vacuum station (model RS-200, HOVAC, Inc.) consisting of an oil-free diaphragm and molecular drag pump was used to attain pressures $\sim 10^{-7}$ Torr ($\sim 2 \times 10^{-5}$ Pa) at the pump inlet. A high accuracy capacitance manometer system (models 120AA/510B combination, MKS Instruments) was used for pressure measurements. Research grade hydrogen and deuterium gases were flowed through a point-of-use chemical filter (Millipore Corporation) prior to entering the Sieverts manifold and reference volumes that had been carefully calibrated. The stainless steel sample container was fully immersed into a fluidized sand bath (Techne Inc.) that was controlled to $\pm 1-2$ K at selected temperatures over the range from 350 to 725 K while the sample materials were exposed to vacuum, the desired hydrogen isotope gas supplies, or reference volumes as needed during activation, desorption, or absorption processes to produce the appropriate stoichiometries for the hydride and deuterides samples.

The preparation procedure started by using a diamond saw to cut pieces of the very hard ZrNi alloy from the ingot. Two "master batches" (i.e., JPL-01 and JPL-13) were made from cleaned and accurately weighed alloy pieces that were then reacted in the JPL Sieverts system with H_2 and D_2 gases, respectively, to their absorption saturation at final pressures over 2.0 bar and with the reactor at ambient (i.e., $\sim$295 K) temperature. After each reaction, the closed reactor vessel was removed from the Sieverts manifold to be opened under purified argon atmosphere in a glove box[17] for removing the now brittle products, which were ground in an agate mortar and pestle until all material passed through a 200-mesh sieve yielding powders with dimensions smaller than 75 μm. After a portion of the hydride product JPL-01 (i.e., $ZrNiH_{2.98}$) was retained for x-ray diffraction (XRD) and NMR measurements, the remainder was returned to the reactor for subsequent desorption of hydrogen by heating to $\sim$675 K under an active vacuum. The resulting ZrNi metal powder (JPL-02) was removed after returning the reactor to the glove box and a portion taken for XRD analysis. Two accurately weighed portions of this ZrNi alloy powder were separately reacted with known quantities of gaseous hydrogen to produce the $ZrNiH_{2.57}$ (JPL-03) and $ZrNiH_{0.85}$ (JPL-04) samples. The remaining ZrNi alloy JPL-02 was sequentially reacted twice with D_2 gas to produce $ZrNiD_{2.64}$ (JPL-05). Two portions of JPL-05 were separately heated to 725 K while being evacuated before reacting with appropriate volumes of D_2 gas to yield $ZrNiD_{1.87}$ (JPL-06) and $ZrNiD_{0.87}$ (JPL-07). Properties of all $ZrNi(H/D)_x$ samples used in the present NMR experiments along with the ZrNi alloy JPL-02 are summarized in Table I. The listed compositions are based upon volumetric determinations of the H_2 (or D_2) gas absorbed during the final reaction step for each sample. Comparison with mass changes following reactions indicate these compositions give x values accurate to within ± 0.02.

In order to establish the phase compositions of all the samples in Table I, powder XRD measurements[9,19] were performed at room temperature using a Siemens D500 diffractometer operating with copper K_α radiation. Each $ZrNi(H/D)_x$ sample was mixed with a small amount of NIST silicon powder as an internal reference material and placed on a cell with a thin window of Kapton film to reduce scattering background. Depending upon stoichiometry and isotope content, essentially all of the XRD peaks for each material in Table I can be assigned to one of the following phases from the International Center for Diffraction Data (Newtown Square, PA 19073-3273, USA) JCPDS files: α-ZrNi (#50-1095); β-$ZrNiH_{1.0}$ (#50-1096); β-$ZrNiD_{1.0}$ (#50-1098); γ-$ZrNiH_{2.7}$ (#50-1097); or γ-$ZrNiD_{2.7}$ (#50-1099). Only sample JPL-06 (i.e., $ZrNiD_{1.87}$) indicated a mixture of the $\beta+\gamma$ phases from the XRD results. As expected from the earlier results of Michel *et al.*[18] on samples from the same ingot, the present XRD patterns for the ZrNi powder (JPL-02) and β-phase hydrides/deuterides contained some weak peaks (i.e., $\leqslant 2\%$) attributable to the Zr_9Ni_{11} intermetallic (i.e., JCPDS file #33-0963) as an impurity phase. These Zr_9Ni_{11} XRD peaks were shifted to slightly lower angles for the γ-phase samples, which is consistent with lattice expansion upon hydrogen/deuterium absorption to form the known solid solution $Zr_9Ni_{11}H_x$ or $Zr_9Ni_{11}D_x$ phases,[20] respectively. However, any more detailed assessment is impossible from the very few and weak peaks for these latter phases. The very low amount of the $Zr_9Ni_{11}(H/D)_x$ should not have any significant influence on the NMR evaluations of the diffusion properties for the dominant β- and γ-$ZrNi(H/D)_x$ phases in these samples. None of the XRD patterns indicate the presence of binary ZrH_x, zirconium oxides, or other Zr-Ni intermetallic phases for any of the samples listed in Table I.

The powder samples were packaged in 5 mm outer diameter borosilicate glass NMR tubes and sealed using a torch under 0.8 atm of N_2 gas. The deuteride samples with $x = 2.98$ and 3.00 were found to support rf eddy currents, as evidenced by changes in the tuning and coupling of the NMR probe circuit when the samples were inserted into the rf coil. To reduce this effect and thereby ensure more complete penetration of the rf field B_1 through the sample, these powders were mixed approximately 1:1 by volume with Al_2O_3 powder. The alumina powder had been dried overnight at 200 °C under vacuum and the mixtures of alumina and metal-deuteride were sealed into new 5 mm tubes. We note that incomplete rf penetration into the sample is expected to decrease the NMR signal/noise ratio but not affect the determinations of T_1 and T_2.

The hydrogen NMR measurements were all at 53.14 MHz in a 1.25 T iron-core electromagnet with F-19 NMR field-stabilization. The deuterium results were obtained primarily at 54.36 MHz in an 8.4 T superconducting solenoid, aug-

TABLE I. Description and properties of the $ZrNiH_x$ and $ZrNiD_x$ that were used in the present NMR experiments. Compositions were obtained from volumetric measurements and phases were identified from powder x-ray diffraction (XRD).

Composition	Sample I.D.	Major $ZrNiH_x$ phases found by XRD	Impurity phases detected by XRD	Predecessor sample I.D. and comments on preparation conditions
$ZrNiH_{2.99}$	JPL-01	γ	$Zr_9Ni_{11}H_x$ ($\sim$1–2%)	First master batch from H_2 with ZrNi metal pieces
$ZrNiH_{2.57}$	JPL-03	γ	—	JPL-02 reacted with H_2
$ZrNiH_{0.85}$	JPL-04	β	Zr_9Ni_{11}	JPL-02 reacted with H_2
$ZrNiD_{3.00}$	JPL-13	γ	$Zr_9Ni_{11}D_x$	Second master batch from D_2 with ZrNi metal pieces
$ZrNiD_{2.98}$	Knox-5	γ	$Zr_9Ni_{11}D_x$ ($\sim$1–2%)	Material originally prepared by Adolphi *et al.* (Ref. 13) and stored
$ZrNiD_{2.64}$	JPL-05	γ	$Zr_9Ni_{11}D_x$	JPL-02 after a 500 K evacuation, reacted with D_2 to give $x=2.93$; a 725 K desorption; and a final reaction with D_2 gas
$ZrNiD_{1.87}$	JPL-06	$\gamma+\beta$	$Zr_9Ni_{11}D_x$	JPL-05 after 725 K desorption and D_2 reaction
$ZrNiD_{0.87}$	JPL-07	β	Zr_9Ni_{11}	JPL-05 after 725 K desorption and D_2 reaction
ZrNi	JPL-02	α	Zr_9Ni_{11}	JPL-01 after 675 K desorption ($x=0.0$)

mented with data at 28.65 MHz in a 4.4 Tesla cryomagnet. Two nearly identical homebuilt rf spectrometers were used, now-standard superheterodyne systems with four rf phases available under transmit and quadrature phase detection for reception.[21] A computer controlled pulse generator was used;[22] the spectrometers were controlled by FIDO software, locally written by Caleb D. Browning and S. S. Gross.

Sample temperatures between 77 K and 293 K were achieved by flowing a stream of nitrogen gas across the sample. The flow of cold nitrogen was maintained through the use of boiler resistors immersed in a 30 L liquid nitrogen storage dewar. The temperature of the gas stream was maintained by a temperature controller regulating a resistive heater in the nitrogen stream. The temperature of the nitrogen gas was measured with a platinum resistance thermometer to provide feedback to the temperature controller. In some cases, sample temperatures were maintained at 77 K by immersing the NMR probe in a glass 4 L liquid nitrogen dewar designed to fit inside the bore tube of the 8.4 T superconducting magnet. Sample temperatures were monitored with a type T thermocouple placed near the NMR coil and sample.

Temperatures greater than 293 K were obtained by winding a noninductive heater on the exterior surface of the copper can of the NMR probe. The heater was regulated with the same temperature controller used for low temperature measurements, with a type E thermocouple placed between the heater windings and the probe for feedback. Again, the sample temperature was monitored with a separate thermocouple placed near the NMR sample. Temperature accuracy of ±1 K and similar temperature regulation stability were more than adequate, given the temperature dependencies of the relaxation times. A maximum safe-temperature limit for each sample was established, based upon concern over the sample disproportionating[8] and upon concern for excessive hydrogen pressure inside the glass sample tubes.[3] These temperature limits are approximately 530 K for $x<2.7$ and 450 K for x near 3.0.

The spin-lattice relaxation times T_1 were measured using the saturation-delay-inspect strategy.[23] The saturation was performed typically by ten $\pi/2$ pulses spaced by 1 ms or twice T_2, whichever was larger. The partially recovered longitudinal magnetization was determined by the amplitude of a free induction decay (FID) following the inspection pulse ($\pi/2$) or of a spin echo generated by two rf pulses.

Measurements of T_2 used FIDs, two-pulse spin echoes, or a train of spin echoes from the CPMG sequence, as discussed in detail below.

III. RESULTS AND DISCUSSION

A. Hydride

The relaxation results for $ZrNiH_x$ are discussed first, because their interpretation is simpler than for the deuteride data. The hydride results are well described by the theory of BPP in which the relaxation is driven by proton-proton dipolar interactions modulated by the H-atom hopping motion.[24,25] We note that chemical shifts of hydrogen cover an approximate range of 10 ppm (530 Hz here). Knight shifts in

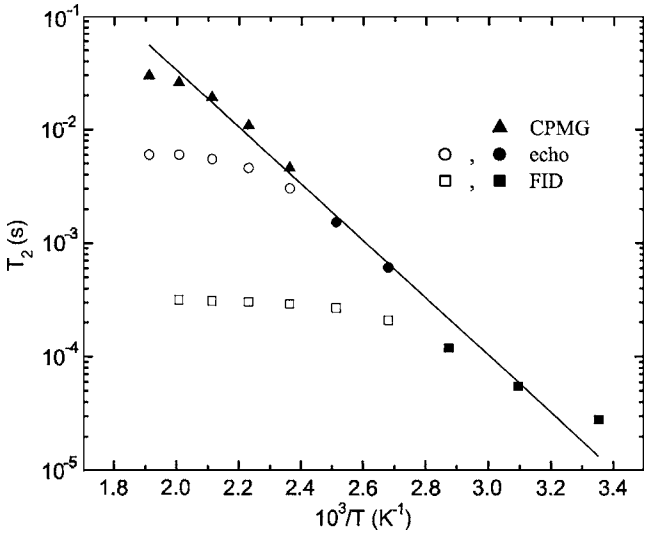

FIG. 1. Temperature dependence of T_2 for $ZrNiH_{0.85}$ by free induction decays (squares), two-pulse spin-echoes (circles), and CPMG echo trains (triangles). The FID values are limited by the static field inhomogeneity and the spin-echo values are limited by effects of diffusion through the susceptibility-induced field gradients. The CPMG data have been extrapolated (slightly) to the limit of zero pulse spacing. The shortest T_2 FID is near the rigid-lattice limit. Filled symbols indicate the T_2 data points selected for use in Fig. 2 and further data analysis.

metal hydrides may exceed this by a factor of about 3. In any event, the shifts are negligible compared to the 20–40 kHz rigid lattice linewidths (FWHM), reflecting the dominant strength of the dipolar interactions.

Overview: At low temperatures, the NMR line attains its rigid lattice width and shape. At higher temperatures, the line narrows and T_2 increases because of motional averaging of the dipolar interactions. At low temperatures, the measured T_1 is dominated by relaxation by conduction electrons, the Korringa mechanism.[14,26] At higher temperatures the relaxation time T_1 decreases below the Korringa value, reflecting the contribution of the dipolar relaxation.

Transverse relaxation: T_2 is measured by different methods, depending on the magnitude of T_2, as presented in Fig. 1 for $ZrNiH_x$ with $x=0.85$. At low temperature, T_2 is small, so the field inhomogeneity caused by the magnetic susceptibility of the sample particles[27] is unimportant. In the region where motional averaging commences, the shape of the FID changes. We have adopted the shape-independent definition,

$$T_2 = \int_0^\infty \frac{g(t)}{g(0)} dt, \tag{1}$$

where $g(t)$ is the FID signal obtained on-resonance. In practice, we use the magnitude value FID to eliminate off-resonance effects, the integral is taken as a sum, and the integral is cut-off at times longer than t_1, where $g(t)$ is essentially zero. Receiver blocking and ringing of the probe tuned circuit after the rf pulse[23] obscure the signal until time t_0, about 5 μs here. So, T_2 is taken as

$$T_2 = \int_{t_0}^{t_1} \frac{|g(t)|}{|g(t_0)|} dt. \tag{2}$$

We note this definition returns the time constant τ for an exponentially decaying signal, $g(t)=\exp(-t/\tau)$.

When the true T_2 has increased sufficiently due to motional averaging, the FID duration is limited by inhomogeneity of the magnetic field,[27] as appears in Fig. 1. The spin echo refocuses this interaction, so T_2 determined from the decay of the echo envelope returns the true T_2,

$$M_{(2\tau)} = M_{(0)} \exp(-2\tau/T_2); \tag{3}$$

typically ten values of τ were used at each temperature. In Fig. 1, the spin echo T_2 increases again with increasing temperature.

At still higher temperatures, where the diffusion D of the hydrogen nuclei has become sufficiently large, there is additional attenuation of the echo amplitude because of diffusion through the nonuniform field in each particle, commonly represented by a gradient G. The echo amplitude becomes[14]

$$M_{(2\tau)} = M_{(0)} \exp(-2\tau/T_2)\exp(-\gamma^2 G^2 D \tau^3 2/3); \tag{4}$$

the extra attenuation is generally mistaken for a shorter T_2 value in Eq. (3). We note that the nonconstant value of G across the sample makes it difficult to separate the linear and cubic terms in τ. Instead, the multiple-echo Carr-Purcell-Meiboom-Gill (CPMG) sequence is used.[14] The amplitude of the nth echo at time $t=2n\tau$ is

$$M_{(t)} = M_{(0)} \exp(-t/T_2)\exp(-\gamma^2 G^2 D \tau^2 t/3), \tag{5}$$

which can be written as

$$M_{(t)} = M_{(0)} \exp(-t/T_2'), \tag{6}$$

where the apparent relaxation rate is

$$\frac{1}{T_2'} = \frac{1}{T_2} + \gamma^2 G^2 D \tau^2/3. \tag{7}$$

The standard analysis is to plot the apparent rate $1/T_2'$ as a function of τ^2; the intercept at $\tau^2=0$ yields the true relaxation rate $1/T_2$. For $ZrNiH_x$, the plots were found to be more nearly linear for $1/T_2'$ against τ itself. Typical τ values were 50, 100, 200, and 500 μs; the extrapolation to $\tau=0$ gave a value of T_2 differing only by a few percent, compared to T_2' at the shortest τ. The CPMG sequence was avoided at lower temperatures where $T_{1\rho}$ is expected to exceed T_2, because the CPMG is known to yield incorrect results there due to spin-locking effects (resulting from cumulative imperfections of the π pulses).[28]

The hydrogen T_2 data in Fig. 1 for $x=0.85$ which are represented by filled symbols were selected as most accurately representing the true relaxation time and appear in Fig. 2 and are used in all further analysis. A similar procedure was used for the γ phase $x=2.57$ data; for $x=2.99$ the region of motional averaging is smaller, so all T_2 data are from FIDs. We note that a clear example of the effects on the apparent T_2 from diffusion through susceptibility-induced field-inhomogeneities in $ZrBe_2H_{1.4}$ has appeared.[29]

Longitudinal relaxation: The measured values of T_1 are

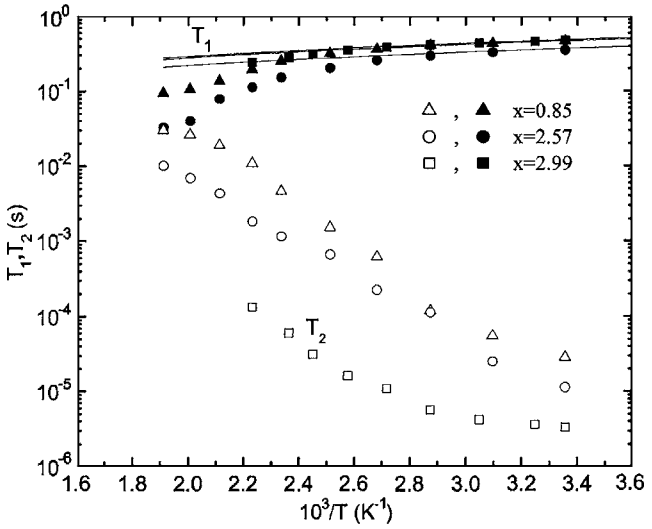

FIG. 2. Measured relaxation times for $ZrNiH_{0.85}$ (triangles), $ZrNiH_{2.57}$ (circles), and $ZrNiH_{2.99}$ (squares). Open symbols indicate T_2 values while closed symbols indicate T_1 values. The light solid curves show the electronic (Korringa) relaxation time T_{1e}, with the Korringa constants listed in Table II.

also presented in Fig. 2. The measured rate $1/T_1$ is the sum of the electronic (or Korringa) contribution $1/T_{1e}$ and the dipolar contribution $1/T_{1d}$. The electronic contribution is expected to be linear in temperature T,[14,26]

$$1/T_{1e} = AT, \tag{8}$$

with the Korringa constant A being determined at low temperatures where the measured T_1 is essentially T_{1e}, as demonstrated by the constancy of T_1 times T. The value of T_{1e} is shown as a light line in Fig. 2 for each sample. The dipolar T_{1d} was then determined as

$$\frac{1}{T_{1d}} = \frac{1}{T_1} - \frac{1}{T_{1e}}. \tag{9}$$

For $x=2.57$ and $x=0.85$, T_1 and T_2 approach equality at the highest temperature examined (see Fig. 2). This indicates that a T_1 minimum (or a peak in $1/T_{1d}$) is not quite attained. To our knowledge, the fact that this occurs just above the maximum safe temperature for both samples is a coincidence.

Second moment: Analysis of the data to obtain mean hopping times τ at each temperature requires knowledge of the second-moment M_2, because this represents the mean-squared dipolar interactions driving the relaxation.[14,25] We obtained M_2 in three independent ways. First, M_2 was taken as

$$M_2 = \frac{\int (\omega - \omega_0)^2 f(\omega) d\omega}{\int f(\omega) d\omega}, \tag{10}$$

with the absorption frequency spectrum $f(\omega)$ coming from the Fourier transform of the magic echo in the low-temperature, rigid-lattice limit. As described elsewhere, the magic echo is essentially the FID signal shifted in time away from the blocking and ringing effects of the rf pulses.[30–32] The ω_0 above is the center frequency of the symmetric resonance line. The integrals in Eq. (10) are performed as discrete sums over the range of frequencies where $f(\omega)$ is not zero. We used the magic-echo sequence $\tau_x \tau_{\bar{x}} (\pi/2)_y$ yielding an echo peak at time τ after the final rf pulse, with $\tau = 15\ \mu$s. This sequence incorporates refocusing of the dephasing due to rf field inhomogeneity; the sequence without refocusing has been shown to yield accurate M_2 values in metal hydrides.[30] In our laboratory, the refocused sequence was thoroughly tested by Brady and found to yield accurate line shapes, even on spectra broader than the present ones (materials with waters of hydration).[33]

A second determination of M_2 is by Van Vleck's lattice sum. For a powder sample, M_2 is given by[14,25]

$$M_2 = \frac{3}{5} \gamma^4 \hbar^2 I(I+1) \sum_k \frac{1}{r_k^6}, \tag{11}$$

where the sum is over all neighbors of the central spin. The lattice sum acquires 99+% of its full value by summing neighbors out to 1.5 nm. For chemically inequivalent nuclei, as in the γ phase, a weighted average across the different types of central spins is performed. We used H-atom coordinates from the neutron diffraction determined crystal structures,[2] as kindly provided by Adolphi. The lattice sum was performed using ATOMS software. For the $x=2.57$ sample, the occupation fraction of each site was taken to be 2.57/3, yielding a second moment smaller by this same fraction than the $x=3$, full occupancy value of M_2.

A third method of determining M_2 comes from the prediction of BPP theory that the geometric mean of T_{1d} and T_2 in a certain regime is independent of the correlation time τ_c (and hence temperature).[24] Specifically,[34] in the slow fluctuation regime $\omega_0 \tau_c \gg 1$,

$$\frac{1}{T_{1d}} = \frac{kM_2}{\omega_0^2 \tau_c}. \tag{12}$$

The measurements do not quite reach the T_1 minimum, so they are always in the slow fluctuation limit, except possibly for the very highest temperature point for each x. In that regime, in the case of motional averaging ($\tau_c < T_{2RL}$ where T_{2RL} is the rigid lattice value of T_2, approximately $1/\sqrt{M_2}$),

$$\frac{1}{T_2} = k' M_2 \tau_c. \tag{13}$$

Thus the geometric mean of T_{1d} and T_2 is[33]

$$\sqrt{T_{1d} T_2} = \frac{\omega_0}{M_2 \sqrt{kk'}}. \tag{14}$$

The constants k and k' are taken from Wolf's lattice-specific calculations.[35] For fcc as used here, $k=1.32$ and $k'=1.15$; the bcc lattice choice (orthorhombic calculations are not available) yields M_2 results within 15% of the fcc result. M_2 is obtained by inverting Eq. (14). We note that the Korringa constants A in Eq. (8) were slightly adjusted to yield a more constant value of $\sqrt{T_{1d} T_2}$; this fine tuning of A was never

TABLE II. Data summary for $ZrNiH_x$.

	M_2 (rad/s)^2 [Eq. (10)] lineshape at low T	M_2 (rad/s)^2 [Eq. (14)] $(T_{1d}T_2)^{1/2}$	M_2 (rad/s)^2 [Eq. (11)] Van Vleck and known structure	E_A (kJ/mol)	τ_0 (s)	Korringa constant A^{-1} (K s)
$ZrNiH_{2.99}$	1.27×10^{10}		1.40×10^{10}	40[a]	2.40×10^{-11}	145
$ZrNiH_{2.57}$	1.26×10^{10}	1.40×10^{10}	1.19×10^{10}	40	1.15×10^{-12}	110
$ZrNiH_{0.85}$	4.01×10^{9}	3.98×10^{9}	2.99×10^{9}	48	7.26×10^{-14}	139

[a]E_A for $x=2.99$ set equal to the value for $x=2.57$.

more than 10%. The light curves in Fig. 2 correspond to the fine-tuned values of A; these are the values in Table II.

All three values of M_2 are reported in Table II. For the $x=2.99$ sample, T_1 remains due primarily to the Korringa mechanism, so the values of T_{1d} obtained are not reliable. Thus, M_2 was not determined from $\sqrt{T_{1d}T_2}$ for this sample. For $x=0.85$ the Van Vleck M_2 is only 75% of the values from magic echo spectra and $\sqrt{T_{1d}T_2}$. This suggests that the hydrogen locations in the neutron-determined structure from Westlake[2] for the β phase are not correct, as was earlier demonstrated by Aldophi from the presence of two deuterium MAS-NMR lines.[13]

Motion analysis: We regard the T_2 data as superior for the calculation of τ_c at each temperature, using Eq. (13). The T_{1d} data are sensitive to the T_{1e} correction of Eq. (9), particularly at lower temperatures where T_1 and T_{1d} are nearly equal. For the analysis, we have used the M_2 values from magic echo spectra in Table II. The mean residence time τ is taken as $2\tau_c$, following the approximation that a jump of either spin of an interacting pair will substantially modulate (decorrelate) the dipolar interaction. The values of τ appear in Fig. 3;

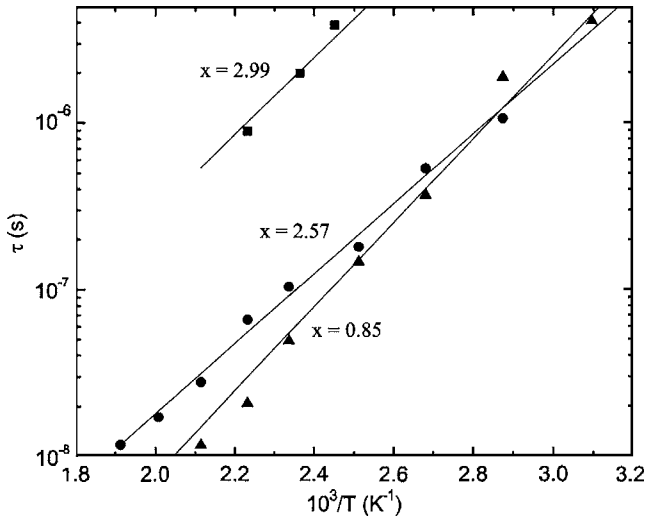

FIG. 3. Temperature dependence of hydrogen residence times τ for $ZrNiH_x$, $x=2.99$ (squares), $x=2.57$ (circles), and $x=0.85$ (triangles). Values of τ were calculated from T_2 data using Eq. (13) and are twice τ_c, as explained in the text. The straight lines are fits to the Arrhenius formula (15) with parameters listed in Table II.

only data with $\tau<4\times10^{-6}$ s (so in the motional averaging region) and $\tau>1.0\times10^{-8}$ s (so in the slow fluctuation limit) are presented.

The values of τ have been fitted to the Arrhenius expression, represented by straight lines in Fig. 3,

$$\frac{1}{\tau}=\frac{1}{\tau_0}\exp\left(\frac{-E_A}{kT}\right), \tag{15}$$

where E_A is the activation energy for H atom hopping and $1/\tau_0$ is the attempt frequency. The parameters E_A and τ_0 are tabulated in Table II. We note that the T_2 data for $x=2.99$ show limited motional averaging, with an overall increase in T_2 of only a factor of about 30. Thus, the τ values in Fig. 3 are inadequate for an independent determination of E_A. Consequently, we used the same activation energy E_A determined for the other γ phase sample, $x=2.57$. The much smaller attempt frequency $1/\tau_0$ for $x=2.99$ is believed to result from the blocking factor, $3-x$. The fraction of sites which are open and hence available to receive an H atom from another site is $(3-x)/3$. The ratio of these factors for $x=2.57$ and 2.99 is 43, though this number may be very inaccurate, resulting as it does from the subtraction of nearly equal quantities (3 and 2.99). Nevertheless, there is reasonable agreement with the ratio (20) of $1/\tau_0$ values from Table II. Thus, the longer τ_0 value for $x=2.99$ apparently results from the blocking factor.

B. Deuteride

The deuteron is a spin-one nucleus with an electric quadrupole moment and a magnetic moment only 15% as large as the proton's. The dipolar contribution to the rigid linewidth is predicted from Eq. (11) to scale as $\sqrt{I(I+1)\gamma^2}$, so a factor of 1/26 as large in the deuterides compared to the hydrides with the same composition x. Given the hydrogen rigid linewidths of 20–40 kHz FWHM, the dipolar broadening in the deuterides is only 0.8–1.5 kHz. The low temperature deuterium spectra in Fig. 4 are much broader than this, so they are primarily quadrupole broadened. We note that these spectra are in agreement with the nonspinning spectra reported by Adolphi *et al.*[13] In particular we note that the present spectrum of the γ phase $x=2.64$ material has two components, from the two kinds of occupied sites (Zr_3Ni and Zr_3Ni_2).

Spectral narrowing: As the deuterium atoms hop through

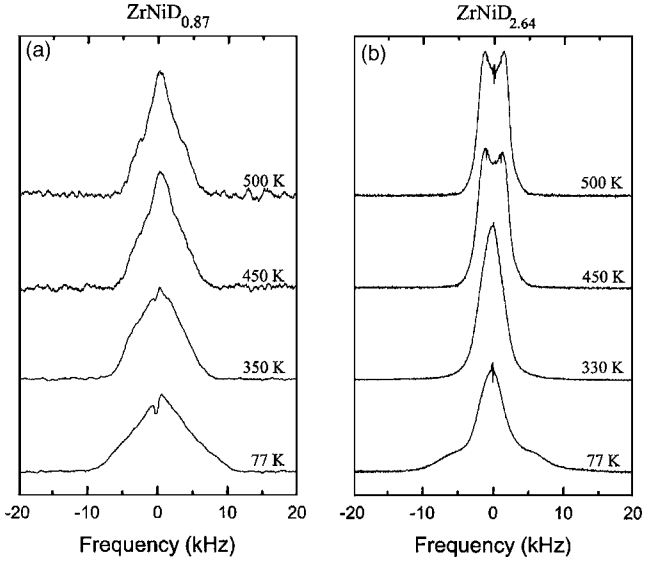

FIG. 4. Line narrowing of (a) $ZrNiD_{0.87}$ and (b) $ZrNiD_{2.64}$ deuterium NMR spectra. At low temperature, $ZrNiD_{2.64}$ consists of two components, a narrow (Zr_3Ni sites) and a broad line (Zr_3Ni_2 sites). Both samples show limited line narrowing, a result of the nonzero electric field gradient averaged over all the sites in the noncubic unit cell.

the lattice, they sample different electric field gradients (EFGs); we note that even at chemically equivalent sites, there will be differently oriented EFG tensors. Thus the result of D-atom hopping at a rate greater than the rigid lattice linewidth is motional narrowing of the resonance line, as evident in Fig. 4. The spectra were obtained from Fourier transforms of echoes formed with a pulse sequence designed to refocus quadrupole interactions for spins one, $(\pi/2)_x-\tau-(\pi/2)_y$. We verified that the largest echo appeared for a refocusing pulse of $\pi/2$, confirming that the primary source of line broadening was electric quadrupolar and not magnetic.

The spectra for both $x=0.87$ and $x=2.64$ appear in Fig. 4 to have attained a limiting (or plateau) line shape for temperatures of 450 K and above. In both cases, the lines are considerably broader than the magnetic field inhomogeneity, which corresponds to a linewidth of 160 Hz FWHM. In detail, the high-temperature hydride linewidth is calculated from the FID data of Fig. 1 and scaled by the ratio of γ_D/γ_H; this procedure makes the reasonable assumption of equal magnetic susceptibilities for the two systems which were gas-loaded from the same ingot of ZrNi. The conclusion is that the quadrupole interactions in $ZrNiD_x$ are reduced by motional averaging, but not to zero. In a noncubic system such as $ZrNiD_x$, there is no symmetry-based reason to expect the average of the EFGs across all available sites to be zero. Indeed, for $x=0.87$ in the β phase, there are four sites, all chemically equivalent according to neutron diffraction. Thus, the four sites should have the same EFG tensors, but differently oriented. Two sites will share one orientation and two sites will have a different orientation, from symmetry considerations. Thus, D atoms will sample only two quadrupole interactions in each cell, so it is not surprising that the $x=0.87$ resonance narrows by only a small amount going from 77 to 500 K. Of course, the true sites occupied in β-$ZrNiD_x$ are unknown, according to the MAS-NMR measurements.[13]

TABLE III. Data summary for $ZrNiD_x$.

	M_2^{hot} [b] $(\text{rad/s})^2$ [Eq. (10)]	M_2^{cold} [b] $(\text{rad/s})^2$ [Eq. (10)]	ΔM_2 [b] $(\text{rad/s})^2$ [Eq. (10)]	Korringa constant A^{-1} (K s)
$ZrNiD_{3.00}$			6.16×10^8 [a]	6150
$ZrNiD_{2.98}$			6.16×10^8 [a]	6150
$ZrNiD_{2.64}$	1.54×10^8	7.70×10^8	6.16×10^8	4700
$ZrNiD_{0.87}$	2.17×10^8	6.63×10^8	4.46×10^8	5900

[a]Set equal to the value for $x=2.64$ in the absence of an independent measurement.
[b]M_2 values and ΔM_2 are primarily of quadrupolar origin.

Second moments: The relaxation processes are driven by motional modulation of the (primarily) quadrupolar spin interactions. Since only part of the second moment M_2 is averaged, the relaxation is driven by ΔM_2,

$$\Delta M_2 = M_{2\ \text{cold}} - M_{2\ \text{hot}}. \tag{16}$$

Here $M_{2\ \text{cold}}$ and $M_{2\ \text{hot}}$ are the limiting (plateau) values,[14] as determined by integration of the spectra, as in Eq. (10). The values are listed in Table III. For $x=2.98$ and 3.00, the extent of motional averaging is inadequate to determine $M_{2\ \text{hot}}$, so ΔM_2 is assumed to be the same as for $x=2.64$.

Mixed phase spectra: One sample of $ZrNiD_x$ has $x=1.87$, placing it squarely in between the β and γ phases at room temperature on the phase diagram. Therefore, the NMR spectrum should be a weighted sum of the spectra from the two phases. To be precise, we should use spectra with the maximum x value of the β phase and the minimum x value of the γ phase, since these x values are at the ends of the phase diagram tie-bar. As we have a limited number of compositions, we take the spectrum for $x=0.87$ to represent the β phase spectrum and $x=2.64$ to represent the γ phase spectrum.

Defining $S(\omega)^{0.87}$ and $S(\omega)^{2.64}$ to be the normalized (unit area) spectra at these concentrations, they correspond to the spectra per unit quantity (e.g., 1 mol) of D atoms. Thus, the predicted normalized spectrum for $x=1.87$ is

$$S(\omega)^{1.87} = fS(\omega)^{0.87} + (1-f)S(\omega)^{2.64}, \tag{17}$$

where f is the fraction of the D atoms in the $x=1.87$ sample residing in the β phase and $1-f$ is the fraction in the γ phase. We let x_β and x_γ be the high and low limiting concentrations in the β and γ phases, respectively. The fractions C_β and C_γ are the fractions of metal atoms in the β and γ phases, respectively. Thus, we have $C_\beta+C_\gamma=1$, $C_\beta x_\beta+C_\gamma x_\gamma=1.87$, $f=C_\beta x_\beta/1.87$, and $1-f=C_\gamma x_\gamma/1.87$. For limiting concentrations $x_\beta=1.1$ and $x_\gamma=2.6$ from the phase diagram,[11] we find $f=0.29$ and $1-f=0.71$.

We inverted Eq. (17) to obtain a predicted normalized spectrum $S(\omega)^{0.87}$, presented as curve (c) in Fig. 5, from the experimental spectra at $x=2.64$ and 1.87. The experimental spectrum at $x=0.87$ is shown as curve (d) and is in excellent

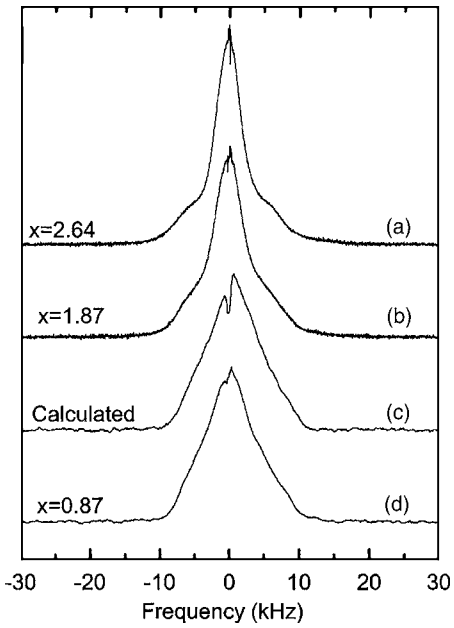

FIG. 5. Experimental deuterium NMR spectrum of the two-phase sample $ZrNiD_{1.87}$ (b). The spectra of the pure γ-phase $ZrNiD_{2.64}$ (a) and β-phase $ZrNiD_{0.87}$ (d) are shown. Spectrum (c) is calculated for $x=0.87$ as the weighted difference between spectra (b) and (a), using $f=0.38$ [Eq. (17)]. A zero-frequency glitch is an instrumental effect in all the spectra.

agreement with the prediction. To obtain curve (c), we used $f=0.38$ and $1-f=0.62$, but values of f between 0.2 and 0.48 gave good agreement. Thus, the experimental spectrum of the $x=1.87$ sample appears to be the weighted sum of its β and γ phase components.

T_1: The measured spin-lattice relaxation times of the $ZrNiD_x$ samples are presented in Fig. 6 for all four samples. The thin curves correspond to the Korringa contributions as in Eq. (8). The Korringa constants are listed in Table III. At high temperatures, particularly for $x=0.87$ and 2.64, the measured T_1 falls below the Korringa curve, showing the motional contribution to the relaxation. Because the Korringa relaxation is purely magnetic, its rate should scale[14] as γ_D^2/γ_H^2 (=1/42.4) for deuteride and hydride samples with the same x. The Korringa constants A^{-1} for the deuterides in Table III were taken from the hydrides in Table II, using the factor of 42.4 and the hydride with most nearly equal composition x. The fits to the data in Fig. 6 are reasonable.

For $x=0.87$ and 2.64, the motional contribution to the measured T_1^{-1} is large. As evident in Fig. 6, the 28.65 MHz data pass through T_1 minima near the highest temperatures studied. These measurements were extended to slightly higher temperatures to ensure capturing the T_1 minima; these measurements were kept short in time to avoid decomposition. Regardless of the details of the relaxation process, at this temperature $\omega_0\tau_c \simeq 1$, so $\tau_c \simeq 5.5\times10^{-9}$ s. Depending on the details of the relaxation model, the minimum T_1 occurs for the product $\omega_0\tau_c$ between 1 and 0.5, so the deduced values of τ_c carry a factor of 2 uncertainty. Because the quadrupole interaction is between a single spin and the fixed lattice (as opposed to a spin-spin interaction as in the hydrides), the mean residence time τ will be equal to τ_c; thus $\tau \simeq 5.5\times10^{-9}$ s at $1000/T=2.1$ K^{-1} for $x=0.87$ and at $1000/T=1.9$ K^{-1} for $x=2.64$. These points approximately agree with the hydride τ values in Fig. 3.

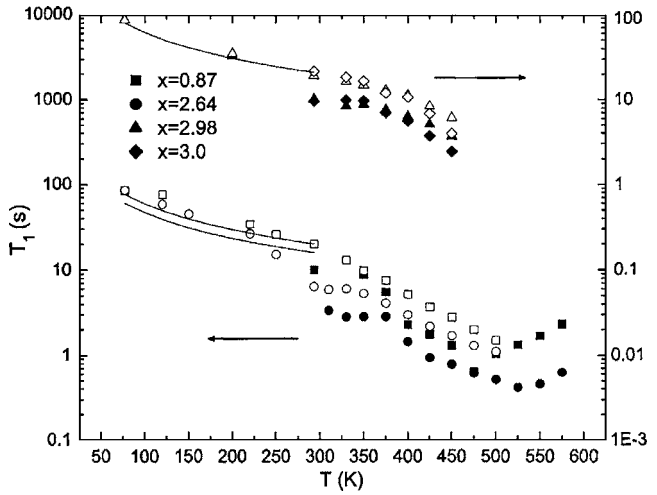

FIG. 6. Deuterium T_1 data from all four samples of $ZrNiD_x$, measured at 54.36 MHz (open symbols) and 28.65 MHz (filled symbols). The light solid curves are the Korringa prediction, with Korringa constants listed in Table III. Note that the $x=2.98$ and 3.0 data are vertically shifted two decades for clarity and use the right-hand vertical scale. For $x=0.87$ and 2.64, T_1 minima are evident at 28.65 MHz at the highest temperatures.

We have obtained activation energies from the T_1 relaxation data for $x=0.87$ and 2.64, after removing the Korringa contribution according to Eq. (9). These T_{1d} data appear in Fig. 7(a), together with straight line (Arrhenius) fits with activation energies $E_A=27$ kJ/mol for $x=0.87$ and $E_A=18$ kJ/mol for $x=2.64$. These deuteride energies are approximately half the energies from the corresponding hydrides listed in Table II. The good agreement of the temperature of the 28.65 MHz T_1 minima with the hydride τ values of Fig. 3 is strong evidence that the motion parameters τ_0 and E_A are actually nearly equal for the hydrides and deuterides. We conclude that the temperature dependence of deuterium T_{1d} data is substantially modified by contributions from another mechanism.

T_2: The deuterium T_2 data provide evidence of corruption by yet another process. Figure 7(b) shows T_2 taken from the decay of two-pulse echoes, $(\pi/2)_x-\tau-(\pi/2)_y$. The low temperature limiting T_2 is reasonable for D-D (like-spin) dipolar coupling, which is only partially refocused by the pulse sequence used. Surprisingly, there is very little motional averaging evident, with the $x=2.64$ and 3.00 data rising only a factor of $\approx$2.5 above the low temperature value. The high temperature T_2 for $x=0.87$ is essentially the same as the low temperature value. We remark that the weak dipole interactions should be fully averaged by the motions at high temperatures and the quadrupolar interactions should be averaged as well (albeit not to zero). Thus, T_2 is expected to rise and eventually become equal to T_1; the two-pulse T_2 data are clearly limited by something else.

Quadrupolar CPMG T_2 data are presented in Fig. 7(c), together with two-pulse T_2 values for $x=0.87$. The CPMG sequence here is the same as the one used for hydrogen, but

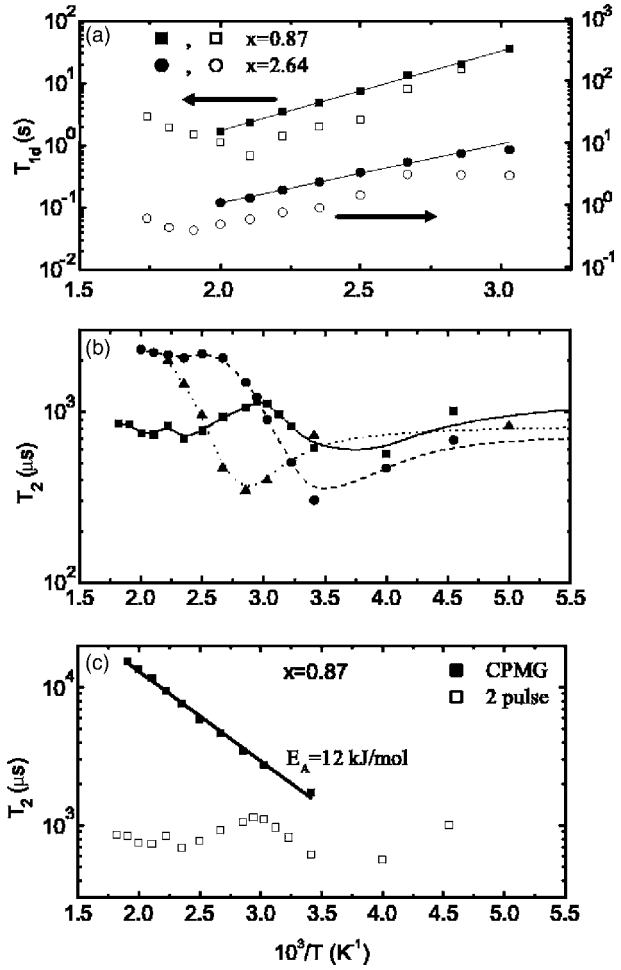

FIG. 7. Temperature dependence of relaxation times T_{1d} (a) and T_2 (b) in $ZrNiD_x$ for $x=3.0$ (triangles), $x=2.64$ (circles), and $x=0.87$ (squares). The T_{1d} data are corrected for Korringa relaxation and the T_2 data are taken from two-pulse spin echo decay envelopes. The solid symbols are T_{1d} data from 54.36 MHz and the open-symbol T_{1d} data were obtained at 28.65 MHz. The T_{1d} at the lower frequency passes through a minimum for both $x=0.87$ and 2.64. The left and right-hand scales refer to $x=0.87$ and 2.64, respectively. The straight lines in (a) are Arrhenius fits to the T_{1d} data. All three samples in (b) show minima in T_2 as a function of temperature where the motion rate is approximately equal to the quadrupolar interaction strength. (c) T_2 data for $x=0.87$ from 2-pulse echoes and from quadrupolar CPMG echo trains. The T_2 data in (b) appear to be limited at high temperatures by an additional relaxation mechanism, as discussed in the text. Uncertainty in each T_2 datum is ±10%.

the refocus pulses are all $\pi/2$. The CPMG data show substantial dependence on the pulse spacing τ and have been extrapolated to $\tau=0$; the extrapolations yield T_2 values differing by as much as 50% from the shortest τ data set ($\tau=50$ μs). Clearly, whatever process restricts the two-pulse T_2 from increasing at high temperatures is at least partially defeated by the frequent refocusing of the CPMG.[36] Nevertheless, the straight line passing through the data corresponds to $E_A=12$ kJ/mol, again much smaller than the energy for the $x=0.85$ hydride. In a broad view, the behavior of the two-pulse data and the CPMG data resemble the effects of diffusion through a field gradient G, as discussed above for the hydrides. However, the effects discussed here for the deuterides are *much* stronger.

We believe that the average electric field gradient over the sites in any one unit cell is not quite constant but varies from cell to cell. As the particle diffuses, it sees large changes in EFG as it hops from site to site. If this were the only time dependent interaction, it would have a correlation time τ (the mean residence time on a given site) and would lead to the expected T_2 behavior, with T_2 rising to meet T_1 at the T_1 minimum, as occurs for the hydride. But there is also a more slowly varying EFG, as the D atom wanders over many unit cells. The cell-to-cell or longer range variations may arise from crystalline imperfections, making each unit cell slightly different. These variations are characterized by correlation times much longer than τ, just as for the variations in B field for a spin diffusing through the inhomogeneous field inside a powder particle. The slow fluctuations lead to additional dephasing; this is most prominent when the fast fluctuations characterized by τ are well averaged. We note that slowly varying spin interactions will defeat the coherent refocusing effect of a spin-echo sequence.[15,16,36]

Disordered systems are often characterized by distributions of correlation times and apparent activation energies from T_1 data in the slow fluctuation limit that are too small. The simple and self-consistent behavior of the hydride data rule out this possibility for $ZrNiD_x$, since the hydride and deuteride were similarly prepared from the same intermetallic ingot.

So what motional information can be taken from the $ZrNiD_x$ data? We present in Fig. 8 specific points showing τ as a function of $1000/T$, together with straight-line (Arrhenius) fits to the hydride data, with parameters from Table II. First, for $x=0.87$ and 2.64, points from the deuterium T_1 minima are presented as stars. Second, there are minima in T_2 (two-pulse) evident in Fig. 7(b); these correspond to a defeat of the coherent refocusing of the rf pulse by the incoherent motions. The T_2 minimum should occur when $\tau=1/\sqrt{\Delta M_2}$, or about 4×10^{-5} s (see Table III). If the quadrupole interaction were substantially changed (~100%) by each jump, we would expect much deeper T_2 minima than appear in Fig. 7(b), with a minimum T_2 of approximately 40 μs. While we have other evidence that the EFG is only weakly modulated by site-to-site motions in the β phase (the small extent of line narrowing in Fig. 4), we do not understand why T_2 does not pass through a deeper minimum for the γ phase samples, $x=2.64$ and 3.00. Points corresponding to the T_1 minima and T_2 minima appear in Fig. 8 as stars.

While the determinations of the D atom τ values and temperatures for the T_1 and T_2 minima have a larger uncertainty than for τ in the hydrides analysis, these data points are located close to the corresponding lines for the hydrides and demonstrate that the motion parameters τ_0 and E_A are at least similar for the hydrides and deuterides. Consequently, the very different activation energies found from the temperature dependencies of T_1 and T_2 in the deuterides are not good measures, as discussed above and immediately below.

We return to the apparent corruption of the deuteride motional relaxation time, T_{1d}. In the present noncubic deuterides, one source of EFG is the metal lattice; these EFGs

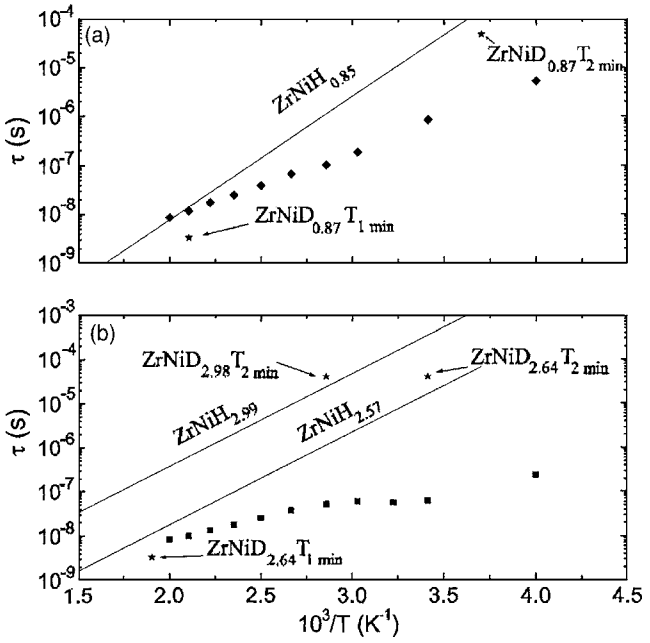

FIG. 8. Temperature dependence of correlation times for $ZrNiD_{2.64}$ (squares), and $ZrNiD_{0.87}$ (diamonds). Deuterium correlation times are calculated from corrected T_1 data using Eq. (12). Deuterium correlation times obtained from T_1 and T_2 minima are shown (stars) as well as fits to the hydride residence time data (solid lines) with similar values of x. Overall, the agreement between the hydrogen results and deuterium T_1 and T_2 minima shows that the hydride and deuteride motion rates are similar. The substantial disagreement with the deuterium results obtained through Eq. (12) is discussed in the text.

fluctuate with characteristic time τ. We speculate that there is an additional fluctuating EFG at a given site, from the motions of neighboring D atoms. Indeed, in those metal deuterides where the D atoms occupy nominally cubic sites, the fluctuating EFGs from moving neighbors are the *only* EFGs.[37,38] In the limit of nearly stoichiometric x values, the additional EFG can be regarded as arising from nearby D-atom vacancies; the relevant correlation time is then the time for a vacancy to move, which is shorter than the mean atomic residence time τ, because the fractional concentration of vacancies is small. Because these EFGs fluctuate at a faster rate than τ^{-1}, when $\omega_0\tau \gg 1$ they may dominate or at least contribute to the quadrupolar relaxation, $1/T_{1d}$. We note that Sholl has shown[39] that the contribution to T_1^{-1} from motions of the neighboring D atoms will vary in magnitude as $c(1-c)$, where c is the D concentration in units where $c=1$ corresponds to fully-filled sites. Neglecting any changes in fundamental hopping rates due to lattice expansion, the temperature dependence of this contribution is independent of concentration c; by comparison, the correlation time τ above depends on c because of site blocking. Thus, as c approaches 1, the strength of the relaxation from EFGs due to neighboring D atoms becomes smaller (fewer D atoms are nearby a vacancy) and the vacancy motion time scale becomes much shorter than τ, so the time scales for modulating the EFGs from D atoms and metal atoms become increasingly separated. If the EFGs from metal atoms and D atoms were known, the approach of Ref. 39 could be used to model the overall relaxation rate.

IV. CONCLUSIONS

Measurements of the spin-lattice and spin-spin relaxation times T_1 and T_2 in the intermetallic compound $ZrNiH_x$ yield a consistent picture, with relaxation well described by the BPP model with a contribution to T_1^{-1} from the conduction electrons. The second moment has been determined by direct integration of magic-echo spectra, by the Van Vleck calculation, and from the geometric mean of T_{1d} and T_2 in the slow fluctuation regime, with good agreement. The H atom mean residence time τ has been calculated from the data at each temperature and activation parameters E_A and τ_0 determined. The $x=2.99$ sample has a much larger τ_0 value than for $x=2.57$, due to site blocking.

The deuterium results for $ZrNiD_x$ display minima in T_1 and T_2, which allow for determination of τ at specific temperatures. These data points indicate that the hydrides and deuterides with similar compositions x have similar τ values (and hence similar E_A and τ_0). Thus, the finding of very much smaller activation energies from the temperature dependencies of the deuterium T_{1d} and T_2 indicate that these analyses are incorrect. We believe that long-range variations in the unit-cell-averaged EFG due to crystal distortions reveal themselves as slowly varying EFGs at a given diffusing D atom. These EFGs lead to shortened dephasing times T_2, because they fluctuate on an intermediate time scale (i.e., both rapidly varying fluctuations and static fluctuations can be fully refocused). Additionally, the EFG at a given D atom may fluctuate not only due to motion of the given atom (with the time constant τ), but to motions of the many neighboring D atoms. Thus, these EFGs will fluctuate with a shorter time constant than τ and may influence the relaxation rate T_1^{-1} in the slow fluctuation regime, confounding the extraction of τ at each temperature.

We believe these results should serve to alert the metal-hydrogen community of possible difficulties in extracting rates of motion from deuterium NMR relaxation data.

ACKNOWLEDGMENTS

The authors wish to thank Mauro Prina and James Kulleck for their assistance with preparation of the hydrides and deuterides at JPL and characterization of all samples by powder x-ray diffraction, respectively. We also thank Natalie Adolphi for valuable discussions and providing the $ZrNiD_{2.98}$ material (i.e., the Knox-5 sample) to us for the present NMR experiments. We appreciate Mike Hartmann's assistance with the crystal structure program. This research was partially supported by NSF Grant No. DMR0400512 and by the Jet Propulsion Laboratory, California Institute of Technology, under a contract with the National Aeronautical and Space Administration.

*Electronic address: msc@wuphys.wustl.edu

[1] D. G. Westlake, J. Less-Common Met. **75**, 177 (1980).
[2] D. G. Westlake, H. Shaked, P. R. Mason, B. R. McCart, M. H. Mueller, T. Matsumoto, and M. Amano, J. Less-Common Met. **88**, 17 (1982).
[3] W. Luo, A. Craft, T. Kuji, H. S. Chung, and T. B. Flanagan, J. Less-Common Met. **162**, 251 (1990).
[4] W. M. Mueller, J. P. Blackledge, and G. G. Libowitz, *Metal Hydrides* (Academic, New York, 1968).
[5] L. Schlapbach, *Hydrogen in Intermetallic Compounds I, Topics in Applied Physics* (Springer-Verlag, Berlin, 1988), Vol. 63.
[6] L. Schlapbach, *Hydrogen in Intermetallic Compounds II, Topics in Applied Physics* (Springer-Verlag, Berlin, 1992), Vol. 67.
[7] R. C. Bowman, Jr., J. W. Reiter, M. Prina, J. G. Kulleck, and W. A. Lanford, in *Proceedings of the International Workshop on Hydrogen in Materials and Vacuum Systems*, edited by G. R. Myneni and S. Chattopadhyay (AIP, New York, 2003), pp. 275–291.
[8] J. S. Cantrell, R. C. Bowman, Jr., L. A. Wade, S. Luo, J. D. Clewley, and T. B. Flanagan, J. Alloys Compd. **231**, 518 (1995).
[9] M. Prina, R. C. Bowman, Jr., and J. G. Kulleck, J. Alloys Compd. **373**, 104 (2004).
[10] K. Watanabe, K. Tanaka, M. Matsuyama, and K. Hasegawa, Fusion Eng. Des. **18**, 27 (1991).
[11] R. Kronski and T. Schober, J. Alloys Compd. **205**, 175 (1994).
[12] P. Dantzer, P. Millet, and T. B. Flanagan, Metall. Mater. Trans. A **32A**, 29 (2001).
[13] N. L. Adolphi, S. Badola, L. A. Browder, and R. C. Bowman, Jr., Phys. Rev. B **65**, 024301 (2001); Phys. Rev. B **69**, 149901(E) (2004).
[14] C. P. Slichter, *Principles of Magnetic Resonance*, 3rd ed. (Springer, New York, 1996).
[15] D. Suwelack, W. P. Rothwell, and J. S. Waugh, J. Chem. Phys. **73**, 2559 (1980).
[16] W. P. Rothwell and J. S. Waugh, J. Chem. Phys. **74**, 2721 (1981).
[17] J. J. Vajo, F. Mertens, C. C. Ahn, R. C. Bowman, Jr., and B. Fultz, J. Chem. Phys. **108**, 13977 (2004).
[18] N. Michel, S. Poulat, P. Millet, P. Dantzer, L. Priester, and M. Gupta, J. Phys. Chem. B **330-332**, 280 (2002).
[19] R. C. Bowman, Jr., S.-J. Hwang, N. L. Adolphi, J. G. Kulleck, and T. J. Udovic (unpublished).
[20] J. M. Joubert, M. Latroche, and A. Percheron-Guegan, J. Alloys Compd. **231**, 494 (1995).
[21] J. D. Ellett, Jr., M. G. Gibby, U. Haeberlen, L. M. Huber, M. Mehring, A. Pines, and J. S. Waugh, in *Advances in Magnetic Resonance*, edited by J. S. Waugh (Academic, New York, 1971), Vol. 5, pp. 117–176.
[22] PulseBlaster from SpinCore Technologies, Inc., Gainesville, FL 32653, USA.
[23] E. Fukushima and S. B. W. Roeder, *Experimental Pulse NMR: A Nuts and Bolts Approach* (Addison-Wesley, Reading, 1981).
[24] N. Bloembergen, E. M. Purcell, and R. V. Pound, Phys. Rev. **73**, 679 (1948).
[25] A. Abragam, *The Principles of Nuclear Magnetism* (Oxford, London, 1961).
[26] J. Korringa, Physica (Amsterdam) **16**, 601 (1950).
[27] L. E. Drain, Proc. Phys. Soc. **80**, 1380 (1962).
[28] M. J. Lizak, T. Gullion, and M. S. Conradi, J. Magn. Reson. (1969-1992) **91**, 254 (1991).
[29] A. F. McDowell, C. F. Mendelsohn, M. S. Conradi, R. C. Bowman, Jr., and A. J. Maeland, Phys. Rev. B **51**, 6336 (1995).
[30] R. C. Bowman, Jr. and W.-K. Rhim, J. Magn. Reson. (1969-1992) **49**, 93 (1982).
[31] W.-K. Rhim, A. Pines, and J. S. Waugh, Phys. Rev. Lett. **25**, 218 (1970).
[32] W.-K. Rhim, A. Pines, and J. S. Waugh, Phys. Rev. B **3**, 684 (1971).
[33] M. R. Hartman, R. Berliner, S. K. Brady, and M. S. Conradi, J. Solid State Chem. **179**, 1259 (2006).
[34] N. Boden, in *The Plastically Crystalline State*, edited by J. N. Sherwood (Wiley, New York, 1979).
[35] D. Wolf, Phys. Rev. B **10**, 2710 (1974).
[36] J. Ph. Ansermet, C. P. Slichter, and J. H. Sinfelt, J. Chem. Phys. **88**, 5963 (1988).
[37] G. Majer, J. Gottwald, U. Kaess, D. T. Peterson, and R. G. Barnes, Phys. Rev. B **68**, 134304 (2003).
[38] W. A. Barton and E. F. W. Seymour, J. Phys. C **18**, 625 (1985).
[39] C. A. Sholl, J. Phys.: Condens. Matter **13**, 11727 (2001).